



Regular Research Manuscript

Synthetic Inertia Provision for Load Frequency Control in Networks with High Penetration of Renewable Energy Sources

Paulina Mkoi[†], Peter M. Makolo, and Francis A. Mwasilu

Department of Electrical Engineering, University of Dar es Salaam, TANZANIA

[†]Corresponding author: paulinamkoi20@gmail.com; ORCID: 0009-0005-0320-3019

ABSTRACT

The integration of renewable energy sources (RESs) such as solar photovoltaic (PV) and wind energy has become a promising solution as the world shifts toward clean energy. Solar PV and wind resources are increasingly replacing conventional synchronous generators, leading to reduced system inertia and increased vulnerability to frequency instability during disturbances. To address this challenge, this study proposes a novel synthetic inertia provision strategy using a battery energy storage system (BESS) integrated alongside solar PV. The proposed method dynamically compensates for the loss of inertia by considering the variability of solar PV output due to changes in irradiance and temperature. Simulation results obtained in MATLAB/Simulink demonstrate that the proposed strategy significantly improves system stability, with a reduction in the rate of change of frequency (RoCoF) by up to 86.6% and an improvement in frequency nadir by 0.91% under high PV penetration scenarios. These results confirm that incorporating synthetic inertia via BESS enhances the frequency response and resilience of low-inertia power systems with high renewable penetration.

ARTICLE INFO

Submitted: **Jan. 5, 2025**

Revised: **Mar. 27, 2025**

Accepted: **Apr. 5, 2025**

Published: **Apr. 2025**

Keywords: *Keywords—Inertia, BESS, RESs, Frequency Response, Frequency Nadir, RoCoF, Solar PV, Synthetic Inertia*

INTRODUCTION

Conventional power systems rely on the inherent inertia of large rotating machines like turbines and synchronous generators in coal, gas, or hydroelectric plants to stabilize the grid frequency during disturbances. This inertia is a direct result of the kinetic energy stored in the rotating masses of synchronous generators and offers a natural resistance to changes in frequency due to sudden imbalances between supply and demand in a power system (Das, 2006; Du et al., 2014; Kundur, 1994; Saadat, 1999; Tielens & Van Hertem, 2016).

This natural resistance slows down the rate of frequency decline or rise, by releasing or absorbing kinetic energy stored in synchronous generators to counteract frequency change (Makolo et al., 2021b). The inertia allows system operators time to react and deploy other control measures, such as primary frequency response or load shedding, to maintain frequency stability.

However, with the increasing penetration of RESs such as solar PV and wind energy into the network, the dynamics of system's frequency are varying significantly. Unlike generator-based sources, RESs are connected to the grid through power electronic

converters. Power electronic converters do not have any rotating mass, hence lack inherent inertia. As a result, the transition towards renewable energy leads to a reduction in the overall system inertia, as more RESs replace generator-based sources (Makolo et al., 2021a, 2021b; Shafiul Alam et al., 2020; Tamrakar et al., 2017; Yap et al., 2019).

As the transition to RESs continues, addressing the challenge of inertia reduction is critical for ensuring the stability of modern power system grids. Various studies have explored synthetic inertia provision using energy storage systems (ESS) and inverter technologies to compensate for the reduced inertia in networks with high penetration of RESs (Cheng et al., 2017; Fang et al., 2018; Kamrul Hasan et al., 2019; Kerdphol et al., 2021; Tedjoe et al., 2019). Grid-forming inverters, such as synchronverters and virtual synchronous generators (VSG), have been widely investigated for their ability to deliver inverter-based synthetic inertia (Du et al., 2021; Jasim & Jasim, 2022; Li et al., 2022; Rubino et al., 2015; Sun et al., 2020; Zhong et al., 2014). However, inverter-based synthetic inertia faces several limitations. The power ratings of inverters restrict the amount of active power that can be injected during frequency events, thereby limiting the system's inertial response. Moreover, the inverters rely on complex control algorithms and signal processing, which are subject to delays and may lead to stability issues if not properly managed. In addition to inverter-based inertia, several works have examined the role of battery energy storage systems (BESS) in providing ESS-based synthetic inertia to enhance frequency stability. BESS can deliver fast inertia support by implementing a synthetic inertia control loop within the converter, as demonstrated in studies (Fang et al., 2018; Kamrul Hasan et al., 2019). This approach has proven effective in mitigating frequency deviations and enhancing system performance during disturbances. While BESS-based synthetic inertia provision has been extensively studied, the integration of RESs, particularly solar PV systems, presents additional challenges due to

their variable and intermittent nature. Since solar PV output power depend solely on irradiance and temperature on the surface of the PV array (Singh, 2013). Previous research has largely focused on BESS in isolation, neglecting the influence of solar PV dynamics on frequency regulation.

In this study, a novel approach is proposed that extends the existing synthetic inertia control strategies by incorporating a solar PV model alongside BESS. The variable nature of solar PV generation is explicitly considered to evaluate the performance and adaptability of synthetic inertia under realistic operating conditions.

This paper, therefore, proposes the provision of synthetic inertia through BESS in networks with high penetration of RESs, specifically inverter-based sources like solar PV. This paper is intended to provide a system with overall high inertia while addressing the variable nature of solar PV.

The remaining parts of this paper are structured as follows: The importance of inertia in power system dynamics in relation to frequency stability is discussed in section 2. Section 3 presents the proposed synthetic inertia provision mechanism. Section 4 presents the results and discussion that validate the performance of synthetic inertia and section 5 concludes the analysis of the research.

CONCEPTUAL FRAMEWORK

Inertia in power system dynamics

The inertia is the first line of defence against frequency change in LFC. It acts immediately following a disturbance in the power system, such as a sudden loss of generation or an increase in load (Makolo et al., 2021, 2024). During a sudden increase in load, the power demand exceeds the power generated hence causing the system frequency to drop. The system releases kinetic energy stored in generator into the system in form of inertia, which helps to slow down the rate of change of frequency (RoCoF). Slowing down the RoCoF helps to bridge the gap between the initial disturbance and provides enough time for other control mechanisms to act and

therefore stabilize the frequency and restore balance in the power system. The relationship between the inertia and frequency change can be illustrated using the swing equation in equation (1).

$$\frac{d\Delta w}{dt} = \frac{1}{2H} (\Delta P_m - \Delta P_e) \quad (1)$$

where, ΔP_m is the change in mechanical power in pu, ΔP_e is the change in electrical power in pu, H is inertia constant and Δw change in system frequency.

The system with minimum inertia has a rapid RoCoF and a high frequency nadir (overshoot after disturbance). The system with high inertia experiences a slower RoCoF and low frequency nadir, which helps to maintain stability. A slower RoCoF means that the system can withstand larger disturbances without tripping protective relays or causing cascading failures (Tielens & Van Hertem, 2016; Ulbig et al., 2014).

Inertia level can be determined based on RoCoF and frequency nadir as shown in Fig. 1 following a load change at time of 5 s.

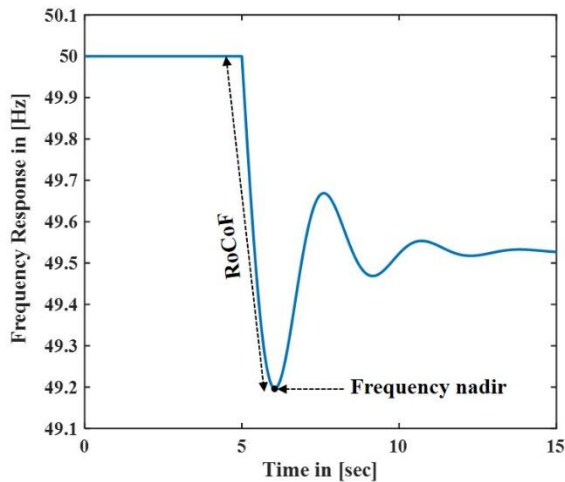


Figure 1: System frequency response under a load disturbance of 0.2 pu at 5s.

THE PROPOSED SYNTHETIC INERTIA PROVISION

This section describes the system layout investigated in this paper as shown in Fig. 2. It consists of a generator-based source, solar PV model integrated into the system through an inverter model and BESS model with an associated converter. The BESS algorithm

receives the frequency change signal from the grid to provide the required synthetic inertia through the associated converter.

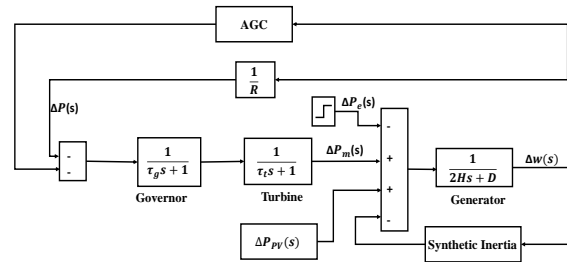


Figure 2: Overall study system.

Generator-based source power system

The generator-based source model, depicted in Fig. 3, represents a conventional power grid dominated by synchronous generators, which serve as the backbone for frequency stability through their inherent mechanical inertia and governor control systems (Das, 2006; Kundur, 1994; Saadat, 1999). The conventional generator model provides a critical baseline for analyzing inertia reduction effects when solar PV systems, are integrated into the network.

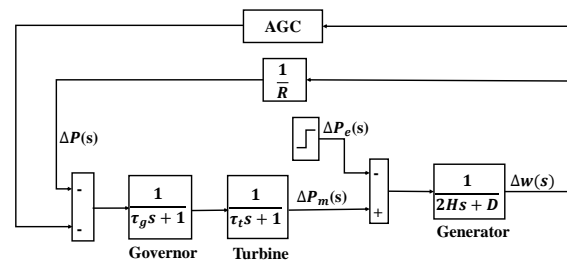


Figure 3: Generator-based source LFC model.

Solar PV model design

The output power of solar PV depends on several environmental and operational factors, mainly solar irradiance (I_r) and ambient temperature ($Temp$) on the surface of the PV array (Singh, 2013). The relationship of PV output power with temperature and irradiance is illustrated in (Annamraju & Nandiraju, 2018; Lee & Wang, 2008; Patel et al., 2020; Vaskov et al., 2022; Yakout et al., 2021) as shown in equation (2).

$$\Delta PV_{out} = PV_{STC} \times \frac{I_r}{I_{rSTC}} \times (1 + \alpha \Delta T) \times \eta \quad (2)$$

where, $\Delta T = Temp - T_{STC}$, ΔPV_{out} is the change in PV output power, STC is standard testing condition, PV_{STC} is PV power at STC, Ir_{STC} is irradiance at STC, Ir is the irradiance, α is the temperature coefficient of PV array, $Temp$ is the temperature, T_{STC} is the temperature at STC and η is output efficiency of MPPT.

Solar irradiance is the dominant factor influencing PV power output, with the power generated by the PV system being directly proportional to the irradiance. However, temperature variations also significantly impact system performance. When the temperature deviates from the Standard Test Condition (STC) value, the PV output adjusts based on the temperature coefficient of the modules (Singh, 2013). As a result, irradiance and temperature determine the actual PV power injected into the system. These variations in PV power influence the system's power balance, leading to fluctuations in frequency hence affecting overall system's frequency stability. The model of output power of PV shown in Fig. 4 is used to integrate the solar PV into power systems. The model enables better forecasting of PV generation, and improve LFC strategies.

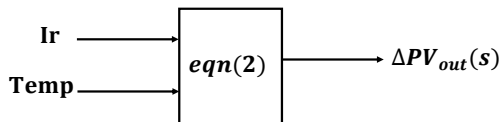


Figure. 4: PV model.

Inverter model design

The inverter model is designed to replicate the response of inverter-based resources in a grid with a high penetration of RESs as shown in Fig. 5. The system includes a PLL, a droop control mechanism, and a power inverter modelled as a first-order system (Pattabiraman et al., 2018).

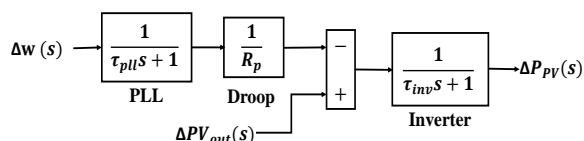


Figure. 5: Inverter model.

Synthetic inertia model design

The design of synthetic inertia is critical in stabilizing power systems with high penetration of RESs, where conventional inertia is reduced. To compensate for the reduced inertia of synchronous generators, synthetic inertia is provided. Synthetic inertia mimics the inertia response of conventional synchronous inertia (Kerdphol et al., 2021). The modified swing equation with synthetic inertia becomes:

$$2H_{eq} \frac{d\Delta w}{dt} = \Delta P_m - \Delta P_e \quad (3)$$

and,

$$H_{eq} = H_{conv} + H_{syn} \quad (4)$$

where H_{eq} is equivalent inertia, H_{conv} is the conventional inertia constant, and H_{syn} is the synthetic inertia constant.

The design of synthetic inertia is based on the derivative control of frequency. The system continuously monitors the RoCoF and reacts accordingly by rapidly injecting or absorbing power through the BESS to balance the grid (Fang et al., 2018; Kamrul Hasan et al., 2019; Kerdphol et al., 2021; Tedjoe et al., 2019).

When the system experiences a sudden frequency decline (under-frequency event), the RoCoF is negative. In response, the BESS discharges (injects) power into the network to arrest the frequency drop. This rapid power injection mimics the release of kinetic energy from conventional synchronous generators, thereby supporting frequency recovery. Conversely, when the system frequency rises above nominal values (over-frequency event), the RoCoF is positive. In this case, the BESS absorbs power from the network by charging its batteries. This absorption slows down the RoCoF. Equations (3) and (4) depict the relationship of BESS power drawn (absorbed or injected) and RoCoF.

$$\Delta P_b = k_b \frac{d\Delta w}{dt} \quad (5)$$

$$\Delta P_b(s) = \frac{1}{1 + \tau_b s} k_b \cdot s \cdot \Delta w(s) \quad (6)$$

where, ΔP_b is the BESS power proportional to H_{syn} , k_b is the BESS capacity, Δw is change in frequency and τ_b is the response time of the associated converter.

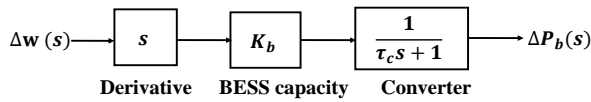


Figure. 6: Synthetic inertia model.

RESULTS AND DISCUSSION

The proposed synthetic inertia provision system's performance is evaluated through simulation studies under different scenarios, including varying PV penetration levels, temperature, irradiance, and load disturbances. Key scientific measurements, including RoCoF and frequency nadir, are analysed to quantify the improvements achieved.

High penetration of solar PV on frequency response

The system frequency response is illustrated for the load increase ($\Delta P_e = 0.2 pu$) at a time of 5 s as shown in Fig. 7. The figure consists of the graph representing a case where the system still has high inertia ($H = 100\%$ in blue trace), and a graph representing a scenario where system inertia is significantly reduced ($H = 40\%$ in red trace) due to high solar PV penetration. The system with high inertia ($H = 100\%$) shows a more controlled response with slow RoCoF ($0.67 Hz/s$) and low frequency nadir ($f = 49.2 Hz$), while the system with low inertia ($H = 40\%$) experiences a much larger frequency deviation, faster RoCoF ($1.25 Hz/s$), a high frequency nadir ($f = 48.75 Hz$) and significant oscillations before settling. As a result, in low inertia system, the RoCoF increases by approximately 86.6%, and the frequency nadir increases by 0.91%.

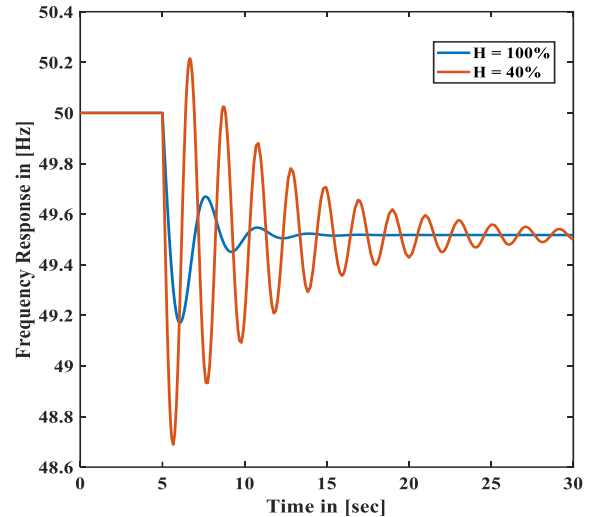


Figure. 7: Frequency response following a load disturbance under high and low inertia scenarios.

Influence of Synthetic Inertia at Different PV Penetration Levels

Test Case 1: Without synthetic inertia

The system is tested under different levels of solar PV power penetration ($P_{PV} = 0.2 pu$, $0.3 pu$, and $0.4 pu$) integrated at a time of 3 s as shown in Fig. 8. For $\Delta P_{PV} = 0.2 pu$ (in blue trace), the frequency nadir is $50.85 Hz$ with a RoCoF of $1.42 Hz/s$. At $\Delta P_{PV} = 0.3 pu$ (in red trace), the frequency nadir is $51.25 Hz$, with a RoCoF increase to $2.5 Hz/s$. The system frequency with the highest PV penetration $\Delta P_{PV} = 0.4 pu$ (in yellow trace) exhibits a faster RoCoF of $3.4 Hz/s$ and the highest frequency nadir ($f = 51.7 Hz$) and largest frequency deviation compared to the systems with low PV power integration ($\Delta P_{PV} = 0.2 pu$ and $0.3 pu$), indicating significantly reduced inertia.

Test Case 2: With synthetic inertia

The same levels of PV power ($\Delta P_{PV} = 0.2 pu$, $0.3 pu$, and $0.4 pu$) were integrated at a time of 3 s, and tested under synthetic inertia. The system response is significantly improved with slower RoCoF, lower frequency nadir, and shorter settling time compared to the system without synthetic inertia, as shown in Fig. 9. For $\Delta P_{PV} = 0.2 pu$ (in blue trace), the frequency nadir is $50.47 Hz$ (reduced from $50.85 Hz$) and RoCoF reduces to $0.26 Hz/s$

(from 1.42 Hz/s). For $\Delta P_{PV} = 0.3$ pu (in red trace), the frequency nadir reaches 50.72 Hz (reduced from 51.25 Hz) with a RoCoF of 0.45 Hz/s (reduced from 2.5 Hz/s), while for $\Delta P_{PV} = 0.4$ pu (in yellow trace), the nadir further improves to 50.93 Hz (from 51.7 Hz) with a RoCoF of 0.62 Hz/s (reduced from 3.4 Hz/s).

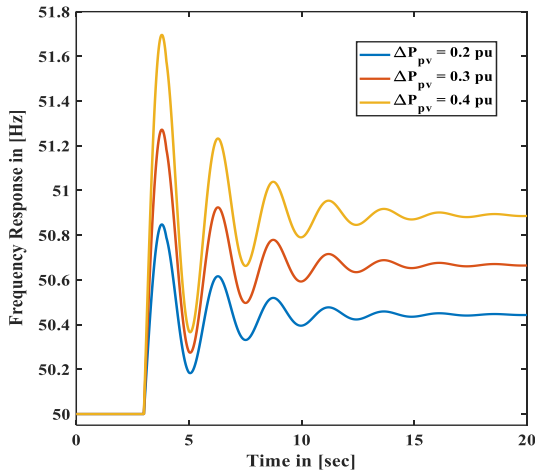


Figure. 8: Frequency response without synthetic inertia under different levels of PV penetration.

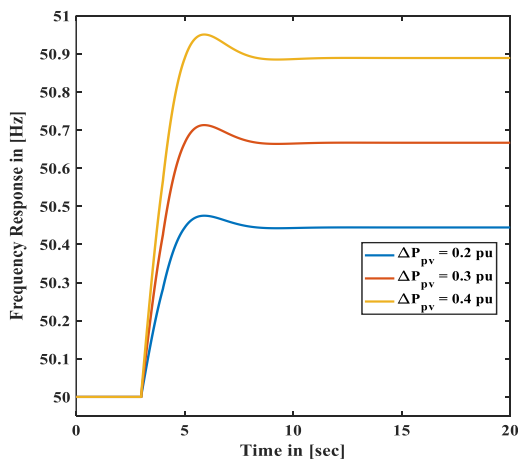


Figure. 9: Frequency response with synthetic inertia under different levels of PV penetration.

Effect of Temperature Variation on Frequency Response

Test Case 1: Without synthetic inertia

The graph in Fig. 10 represents a system with low inertia due absence of synthetic inertia, with different temperatures ($Temp = 10$ °C, 25 °C, and 40 °C) on the PV array surface at time 3 s. The system with the lowest

temperature ($Temp = 10$ °C) shows the highest frequency nadir of 52.15 Hz and the highest RoCoF of 2.15 Hz/s, due to higher PV power output, contributing to a large frequency deviation. The system at $Temp = 25$ °C exhibits a frequency nadir of 51.9 Hz and a RoCoF of 1.9 Hz/s. The system at $Temp = 40$ °C shows a frequency nadir of 51.75 Hz and a RoCoF of 1.75 Hz/s, indicating a progressively slower RoCoF and lower overshoot with increasing temperature.

Test Case 2: With synthetic inertia

The same temperature variations ($Temp = 10$ °C, 25 °C, and 40 °C) are considered in Fig. 11. With synthetic inertia, the system frequency response is significantly improved. The RoCoF is slower, and the frequency nadir is reduced compared to the system without synthetic inertia. For $Temp = 10$ °C, the frequency nadir is 51.19 Hz (reduced from 52.15 Hz), and the RoCoF is 1.08 Hz/s (reduced from 2.15 Hz/s). At $Temp = 25$ °C, the frequency nadir is 51.02 Hz (reduced from 51.9 Hz) with a RoCoF of 0.93 Hz/s (down from 1.9 Hz/s). For $Temp = 40$ °C, the frequency nadir reaches 50.93 Hz (reduced from 51.75 Hz), and the RoCoF drops to 0.84 Hz/s (reduced from 1.75 Hz/s). These results confirm that synthetic inertia enhances frequency stability by slowing down the RoCoF and reducing the frequency nadir after a disturbance.

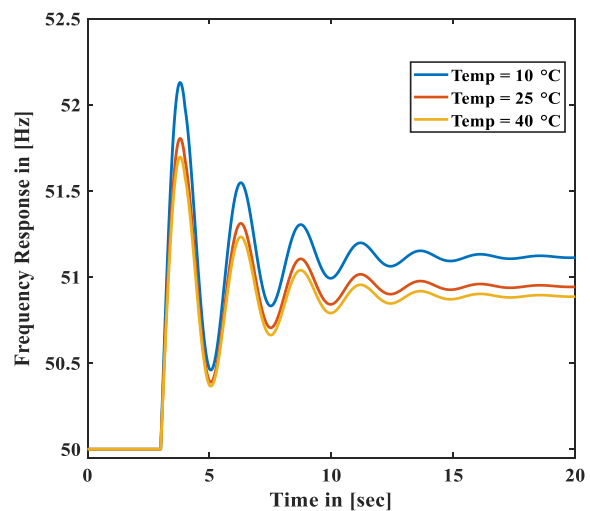


Figure. 10: Frequency response with varying PV temperature without synthetic inertia.

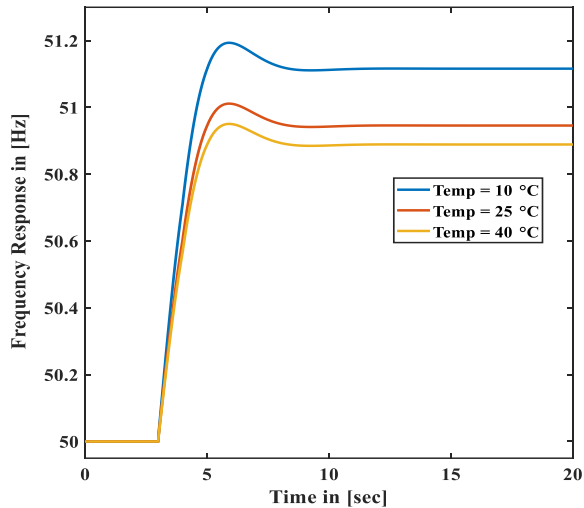


Figure. 11: Frequency response with varying PV temperature with synthetic inertia.

Effect of irradiance variation on frequency response

Test Case 1: Without synthetic inertia

Fig. 12 illustrates the frequency response due to irradiance variation ($I_r = 0 \text{ W/m}^2$, 300 W/m^2 , 700 W/m^2 , and 1000 W/m^2) on the surface of the PV array at a time of 3 s. The system with the highest irradiance ($I_r = 1000 \text{ W/m}^2$) experiences a rapid RoCoF of 1.8 Hz/s and the highest frequency nadir of 51.8 Hz . This is because PV power is directly proportional to irradiance, high irradiance results in a larger power injection, causing a greater disturbance to the system. At $I_r = 700 \text{ W/m}^2$, the frequency nadir is 51.25 Hz and the RoCoF is 1.25 Hz/s , while at $I_r = 300 \text{ W/m}^2$, the nadir drops to 50.55 Hz with a RoCoF of 0.55 Hz/s . For $I_r = 0 \text{ W/m}^2$, the PV power output is zero, meaning the solar PV does not contribute any power to the system. These results indicate that higher irradiance leads to more frequency deviation and faster RoCoF due to the sudden increase in PV power output.

Test Case 2: With synthetic inertia

The benefits of incorporating synthetic inertia into the system are demonstrated in Fig. 13, considering irradiance variation similar to Case 1. The frequency response is more stable, with slower RoCoF, lower frequency

nadir, smaller deviations, and shorter settling time compared to the system without synthetic inertia. For $I_r = 1000 \text{ W/m}^2$, the frequency nadir is 51 Hz (reduced from 51.8 Hz), and the RoCoF is 0.5 Hz/s (reduced from 1.8 Hz/s). At $I_r = 700 \text{ W/m}^2$, the frequency nadir is 50.7 Hz (reduced from 51.25 Hz), and the RoCoF is 0.35 Hz/s (reduced from 1.25 Hz/s). For $I_r = 300 \text{ W/m}^2$, the nadir is 50.3 Hz (down from 50.55 Hz), and the RoCoF drops to 0.15 Hz/s (reduced from 0.55 Hz/s). These improvements confirm the positive impact of synthetic inertia in enhancing system frequency stability under varying irradiance conditions.

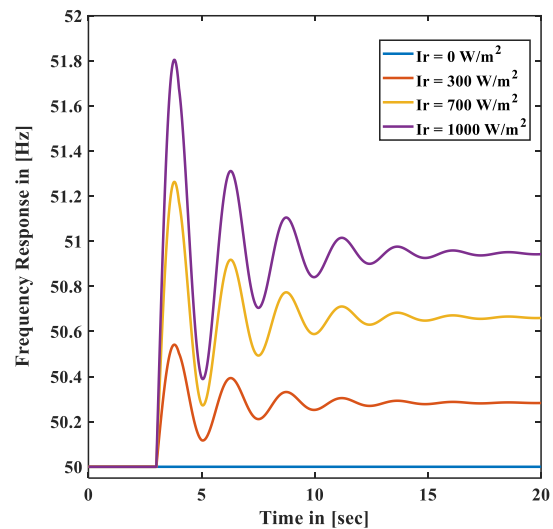


Figure. 12: Frequency response with varying PV irradiance without synthetic inertia.

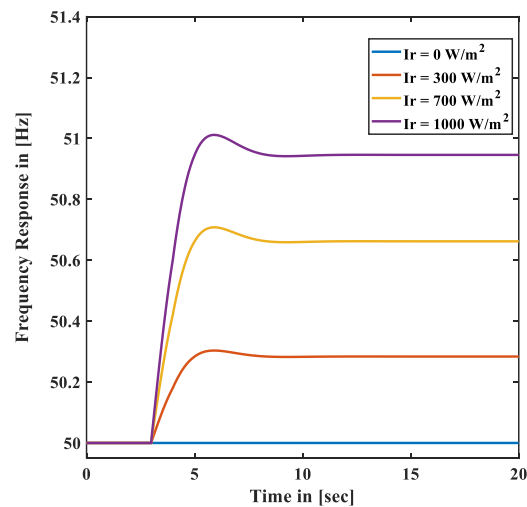


Figure. 13: Frequency response with varying irradiance with synthetic inertia.

Effects of Varying Synthetic Inertia Values on Frequency Response

Synthetic inertia provides a control mechanism that mimics the inertial response provided by synchronous generators. High values of synthetic inertia indicate that a system has high overall inertia while, low synthetic inertia values indicate that a system has low overall inertia. The value of synthetic inertia depends on the capacity of BESS. The frequency response is analyzed for different values of synthetic inertia ($k_b = 5\%$, 15% , 20% and 30%).

In Fig. 14, at a time of 3 s, PV power ($\Delta P_{PV} = 0.4 pu$) is integrated into the system. A system with low synthetic inertia ($k_b = 5\%$) experiences a highest frequency nadir of 51.30 Hz and a fast RoCoF of 0.65 Hz/s, indicating that the system has low overall inertia. As synthetic inertia increases, the system response improves. For $k_b = 15\%$, the frequency nadir is 51.05 Hz and the RoCoF is 0.53 Hz/s. At $k_b = 20\%$, the nadir is 51.00 Hz, and RoCoF reduces to 0.50 Hz/s. With high synthetic inertia $k_b = 30\%$, the system experiences the lowest frequency nadir of 50.95 Hz and the slowest RoCoF of 0.48 Hz/s (26.15% decrease compared to $k_b = 5\%$ case), resulting in shorter settling time due to the increased overall system inertia.

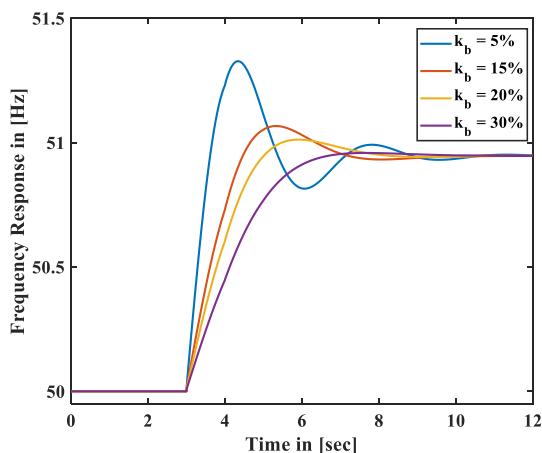


Figure. 14: Solar PV integration of 0.4 pu at 3 s with varying synthetic inertia values.

In Fig. 15, at a time of 10 s, a load change ($\Delta P_e = 0.2 pu$) is introduced into the system. When synthetic inertia is low inertia ($k_b =$

5%), the system exhibits a highest frequency nadir of 49.28 Hz and fast RoCoF of 0.72 Hz/s, along with prolonged oscillations indicating low overall inertia. However, as synthetic inertia increases, the system performance improves significantly. For $k_b = 15\%$, the frequency nadir is reduced to 49.45 Hz, and the RoCoF decreases to 0.55 Hz/s.

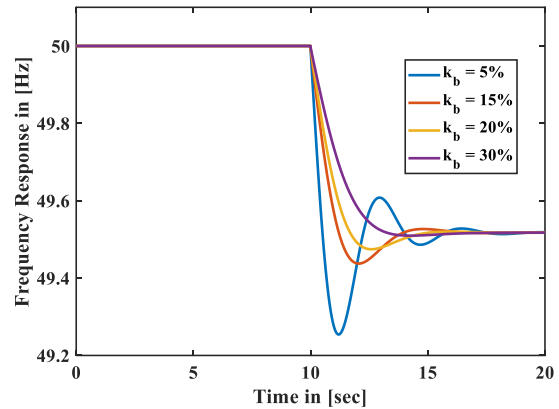


Figure. 15: Load disturbance of 0.2 pu at 10 s with varying synthetic inertia values.

Further increasing synthetic inertia to $k_b = 20\%$ results in a frequency nadir of 49.50 Hz and a RoCoF of 0.50 Hz/s. With the highest synthetic inertia $k_b = 30\%$, the system achieves the best response with frequency nadir improves to 49.58 Hz, and the RoCoF reduces to 0.42 Hz/s (41.7% decrease compared to the $k_b = 5\%$ case).

Overall System Behaviour with and without Solar PV Integration

The graphs in Fig. 16 and Fig. 17 represents a system with synthetic inertia when a load changes ($\Delta P_e = 0.2 pu$) occur at a time of 10 s and ($\Delta P_e = 0.3 pu$) occur at a time of 15 s. Following the disturbances, the system shows slow RoCoF, low frequency nadir, small frequency deviation and oscillation with shorter settling time due to high overall inertia.

In Fig. 16, the PV power injected into the system is zero ($P_{PV} = 0$ in red trace) meaning the system is supplied by synchronous generators. At a time of 10 s when an increase of load ($\Delta P_e = 0.2 pu$) occurs, the synchronous generators increase generation

by ($\Delta P_m = 0.2 pu$) to balance with the demand. At a time of 15 s when again a load increase of ($\Delta P_e = 0.3 pu$) is introduced into the system, synchronous generators increase generation by ($\Delta P_m = 0.2 pu$). At this time the total load change is $0.5 pu$ equivalent to synchronous generators generation.

In Fig. 17, at a time of 3 s, the solar PV power ($P_{PV} = 0.4 pu$) is integrated into the system, which replaces the synchronous generators ($\Delta P_m = 0.4 pu$) to balance between generation and demand. Although the solar PV replaces part of the synchronous generation, the remaining synchronous generators are operated at reduced capacity in such a way that they can adjust their output to respond to system demand variations. At a time of 10 s when an increase of load ($\Delta P_e = 0.2 pu$) occurs, the synchronous generators increase generation by ($\Delta P_m = 0.2 pu$) to balance with the demand. Since it is difficult to adjust the generation of PV power to accommodate an extra load, synchronous generators are used. At a time of 15 s, when again a load increase of ($\Delta P_e = 0.3 pu$) is introduced into the system, synchronous generators increase generation by ($\Delta P_m = 0.3 pu$).

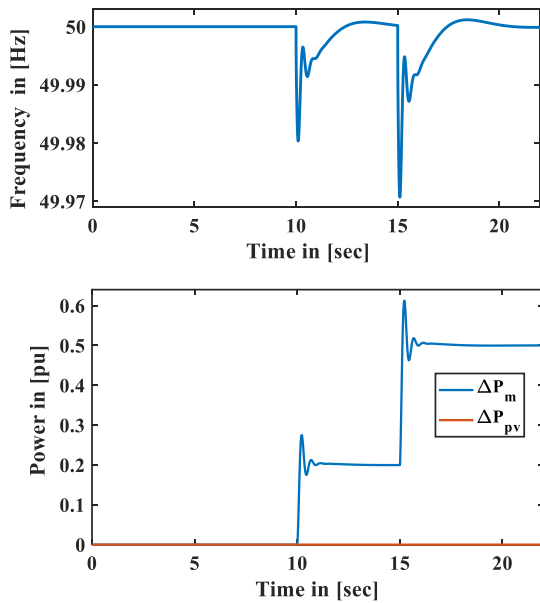


Figure. 16: Overall system response without solar PV.

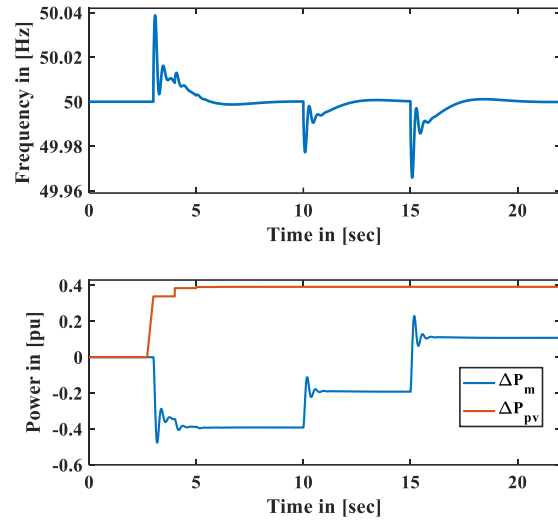


Figure. 17: Overall system response with solar PV.

BESS sizing

Size of the BESS required depends on the synthetic inertia (H_{syn}) needed to compensate for the loss of inertia due to PV integration to ensure that the system has high overall targeted inertia (H_{eq}). The overall targeted inertia should enable the system to experience, slow RoCoF and low frequency nadir after disturbances to maintain frequency stability similar to conventional network.

Through simulation the value of k_b is used to estimate the required size of the BESS. From the simulations, BESS with capacity ($k_b = 20\%$) is used to provide synthetic inertia, $k_b = 20\%$ means that the BESS can inject or absorb power equal to 20% of plant capacity. The following steps are used to determine the actual value of the BESS size.

- (i) Estimation of BESS power as shown below using equations (7) and (8)

$$P_b = 20\% \times P_c \quad (7)$$

$$P_b = 0.2 \times 200 \text{ MW} = 40 \text{ MW} \quad (8)$$

where, P_b is BESS power and P_c is plant capacity power.

- (ii) Estimation of BESS energy required to provide synthetic inertia, duration of inertia response (10 s) is used to determine the energy of BESS as shown in equations (9) and (10).

$$E_b = P_b \times t_{in} \quad (9)$$

$$E_b = 40 \text{ MW} \times 10 \text{ s} = 400 \text{ MJ} \quad (10)$$

where, E_b is BESS energy and t_{in} is inertia response time.

(iii) Battery size in kWh is shown in equation (11)

$$B_s = 400 \times \frac{10^3}{3.6 \times 10^3} = 111.1 \text{ kWh} \quad (11)$$

where B_s is the battery size. Therefore, the size of BESS required to provide the synthetic inertia in order for the system to have high overall inertia is approximately to 120 kWh.

CONCLUSION

This research presented synthetic inertia provision by BESS for networks with high penetration of RESs, particularly solar PV. The integration of solar PV alongside synthetic inertia presents a significant step towards developing resilient frequency control strategies in modern power systems. Upon integration of PV into the system, the generator's inertia and damping values were reduced, corresponding to the percentage of PV penetration to indicate the reduction in inertia due to the replacement of a generator-based system by an inverter-based system. The BESS was observed, that it can provide the synthetic inertia required to make up for the loss of inertia, resulting in a system with high overall inertia regardless of the penetration of PV power into the system. Through simulating various scenarios with fluctuating solar generation were considered to achieve the objective of this research. The synthetic inertia directly supplements the system's total inertia, effectively slowing RoCoF and improving system stability during disturbances.

This work provides deeper insight into the interaction between RESs generation variability and synthetic inertia performance. The BESS in this research is used only for inertia provision, but the BESS can also be used as backup power, especially when the solar PV power is almost zero when the irradiance is zero. The frequent charge-discharge cycles required for effective synthetic inertia provision can accelerate battery degradation, reducing lifespan and increasing replacement costs. Considering the costs of BESS and their lifespans, more research is needed on how to utilize both inverter-based and BESS-based synthetic

inertia provision to improve the lifespan of BESS.

APPENDIX

The data used in this research are shown in Table 1.

Table 1: Data used

Parameter	Value
System frequency	$f = 50 \text{ Hz}$
Governor time constant	$\tau_g = 0.2 \text{ s}$
Turbine time constant	$\tau_t = 0.5 \text{ s}$
Inertia constant before PV integration	$H = 4 \text{ s}$
Inertia constant after PV integration	$H_{conv} = 2.4 \text{ s}$
Governor speed regulation	$R = 0.050$
Damping constant	$D = 1.2$
Battery time constant	$\tau_b = 0.02 \text{ s}$
Temperature at STC	$T_{STC} = 25^\circ\text{C}$
Plant capacity	$P_c = 200 \text{ MW}$
Irradiation at STC	$I r_{STC} = 1000 \text{ W/m}^2$
PV power at STC	$PV_{STC} = 0.4 \text{ pu}$
Inverter droop	$R_d = 0.05$
Battery capacity	$k_b = 20\%$
PV efficiency	$\eta = 0.95$
Temperature coefficient	$\alpha = -0.004/^\circ\text{C}$
PLL time constant	$\tau_{pll} = 0.1 \text{ s}$
Inverter time constant	$\tau_{inv} = 0.5 \text{ s}$
Base power	$P = 200 \text{ MW}$

REFERENCES

- Annamraju, A., & Nandiraju, S. (2018). Robust Frequency Control in an Autonomous Microgrid: A Two-Stage Adaptive Fuzzy Approach. *Electric Power Components and Systems*, **46**(1), 83–94. doi:10.1080/15325008.2018.1432723
- Das, D. (2006). *Electrical Power System*. New Age International (P) Ltd., Publishers All.
- Du, W., Tuffner, F. K., Schneider, K. P., Lasseter, R. H., Xie, J., Chen, Z., & Bhattacharai, B. (2021). Modeling of Grid-Forming and Grid-Following Inverters for Dynamic Simulation of Large-Scale Distribution Systems. *IEEE Transactions on Power Delivery*, **36**(4), 2035–2045. doi:10.1109/TPWRD.2020.3018647

- Fang, J., Tang, Y., Li, H., & Li, X. (2018). A Battery/Ultracapacitor Hybrid Energy Storage System for Implementing the Power Management of Virtual Synchronous Generators. *IEEE Transactions on Power Electronics*, **33**(4), 2820–2824. doi:10.1109/TPEL.2017.2759256
- Jasim, A. M., & Jasim, B. H. (2022). Grid-Forming and Grid-Following Based Microgrid Inverters Control. *Iraqi Journal for Electrical and Electronic Engineering*, **18**(1), 111–131. <https://doi.org/10.37917/ijeee.18.1.13>
- Kamrul Hasan, A. K. M., Haque, M. H., & Aziz, S. M. (2019). Application of battery energy storage systems to enhance power system inertia. *2019 29th Australasian Universities Power Engineering Conference, AUPEC 2019*. doi:10.1109/AUPEC48547.2019.211941
- Kerdphol, T., Rahman, F. S., Watanabe, M., & Mitani, Y. (2021). Virtual Inertia Synthesis and Control. In *Power Systems*. <https://link.springer.com/book/10.1007/978-3-030-57961-3-030-57961-6>
<http://link.springer.com/10.1007/978-3-030-57961-6>
- Kundur, P. (1994). Power System Stability and Control. In *Power System Stability and Control*. McGraw- Hill Companies, Inc. doi:10.1201/9781420009248
- Lee, D. J., & Wang, L. (2008). Small-signal stability analysis of an autonomous hybrid renewable energy power generation/energy storage system part I: Time-domain simulations. *IEEE Transactions on Energy Conversion*, **23**(1), 311–320. doi:10.1109/TEC.2007.914309
- Li, Y., Gu, Y., & Green, T. C. (2022). Revisiting Grid-Forming and Grid-Following Inverters: A Duality Theory. *IEEE Transactions on Power Systems*, **37**(6), 4541–4554. doi:10.1109/TPWRS.2022.3151851
- Makolo, P., Zamora, R., & Lie, T. T. (2021). The role of inertia for grid flexibility under high penetration of variable renewables - A review of challenges and solutions. *Renewable and Sustainable Energy Reviews*, **147**, Article 111223. doi:10.1016/j.rser.2021.111223
- Makolo, P., Zamora, R., Perera, U., & Lie, T. T. (2024). Flexible Synthetic Inertia Optimization in Modern Power Systems. *Inventions*, **9**(1), 1–18. doi:10.3390/inventions9010018
- Patel, S., Mohanty, B., & Hasanien, H. M. (2020). Competition over resources optimized fuzzy TIDF controller for frequency stabilization of hybrid micro-grid system. *International Transactions on Electrical Energy Systems*, **30**(9), 1–20. doi:10.1002/2050-7038.12513
- Pattabiraman, D., Lasseter, R. H., & Jahns, T. M. (2018). Comparison of Grid Following and Grid Forming Control for a High Inverter Penetration Power System. *2018 IEEE Power & Energy Society General Meeting (PESGM)*, 1–5. doi:10.1109/PESGM.2018.8586162
- Rubino, S., Mazza, A., Chicco, G., & Pastorelli, M. (2015). Advanced control of inverter-interfaced generation behaving as a virtual synchronous generator. *2015 IEEE Eindhoven PowerTech, PowerTech*. doi:10.1109/PTC.2015.7232753
- Saadat, H. (1999). *Power System Analysis*. McGraw- Hill Companies, Inc.
- Singh, G. K. (2013). Solar power generation by PV (photovoltaic) technology: A review. *Energy*, **53**, 1–13. doi:10.1016/j.energy.2013.02.057
- Sun, D., Liu, H., Gao, S., Wu, L., Song, P., & Wang, X. (2020). Comparison of Different Virtual Inertia Control Methods for Inverter-based Generators. *Journal of Modern Power Systems and Clean Energy*, **8**(4), 768–777. doi:10.35833/MPCE.2019.000330
- Tedjoe, P. A., Ally, C. Z., & De Jong, E. C. W. (2019). Analysis of battery-based virtual inertia primary frequency response on improving frequency dynamics in an island hydro-diesel-PV ac-grid. *2019 IEEE 60th Annual International Scientific Conference on Power and Electrical Engineering of Riga Technical University, RTUCON 2019 - Proceedings*. doi:10.1109/RTUCON48111.2019.8982338
- Tielens, P., & Van Hertem, D. (2016). The relevance of inertia in power systems. *Renewable and Sustainable Energy Reviews*, **55**, 999–1009. doi:10.1016/j.rser.2015.11.016
- Ulbig, A., Borsche, T. S., & Andersson, G. (2014). Impact of low rotational inertia on power system stability and operation. *IFAC Proceedings Volumes (IFAC-PapersOnline)*, **19**, 7290–7297. doi:10.3182/20140824-6-za-1003.02615
- Vaskov, A. G., Mozder, N. Y., & Narynbaev, A. F. (2022). Modelling of Solar-Diesel Hybrid

Power Plant. *IOP Conference Series: Materials Science and Engineering*, **1211**(1), 012011. doi:10.1088/1757-899x/1211/1/012011

Yakout, A. H., Kotb, H., Hasanien, H. M., & Aboras, K. M. (2021). Optimal Fuzzy PIDF Load Frequency Controller for Hybrid Microgrid System Using Marine Predator Algorithm. *IEEE Access*, **9**, 54220–54232. doi:10.1109/ACCESS.2021.3070076

Zhong, Q. C., Nguyen, P. L., Ma, Z., & Sheng, W. (2014). Self-synchronized synchronverters: Inverters without a dedicated synchronization unit. *IEEE Transactions on Power Electronics*, **29**(2), 617–630. doi:10.1109/TPEL.2013.2258684